

Semiconducting B–C–N nanotubes with few layers

D. Golberg ^{*}, P. Dorozhkin ¹, Y. Bando, M. Hasegawa, Z.-C. Dong

National Institute for Materials Science, Namiki 1-1, Tsukuba, Ibaraki 305-0044, Japan

Received 19 February 2002; in final form 27 March 2002

Abstract

Perfectly ordered nanotubes (NTs) displaying a limited number of defect-free B–C–N shells (typically 2–4) were synthesized from CVD C NTs and a mixture of boron oxide and gold oxide placed in a flowing N₂ atmosphere at ~1950 K. The NTs were analyzed using field emission conventional and energy-filtered (Omega filter) high-resolution electron microscopes, and electron energy loss and energy dispersive X-ray spectrometers. NTs with inner diameters of 0.9–4.0 nm were frequently assembled in bundles consisting of several tubes and extending up to 1–2 μm in length. Two-terminal transport measurements on individual B–C–N nanotube bundles were carried out in-situ in a Fresnel projection microscope. The bundles displayed semiconducting behavior with an estimated band gap of ~1 eV. © 2002 Published by Elsevier Science B.V.

1. Introduction

In addition to C nanotubes (NTs) [1], extensively studied over the last decade, NTs may form in the B–C–N system [2–17]. The structures of graphite and hexagonal BN are nearly identical (unit cell, atomic distances), making the ternary B–C–N NTs a unique material due to the possibility of random and/or ordered substitution of B and N atoms for C atoms in the graphitic sheet. Moreover, the conduction properties of C NTs and those of BN are predicted to be diametrically opposite. C NTs are known to be metals or semi-

conductors [18], while BN NTs are expected to be insulators [19]. So preparation of ternary B–C–N NTs of various compositions may allow one to tune transport properties over a wide range.

Control of the number of layers grown for a given NT is an important issue as far as electronic applications are concerned. It has been shown that transport properties of C NTs are a complex function of the number of graphitic shells, wall defects, diameter, helicity and cross-sectional shape [18,20]. Clearly, the smaller the number of tube layers, the fewer topological defects affecting the electron transport are introduced into the graphitic network. Thus, for real applications, NTs with few layers are advantageous. In C, bundles of single-walled NTs [21] as well as double-walled NTs [22] have been synthesized. In BN, double-walled morphology has also been observed [23–25]. There have been a few reports on synthesis of single-walled BN NTs [12,13,26,27]. By

^{*} Corresponding author. Fax: +81-298-51-6280.

E-mail address: golberg.dmitri@nims.go.jp (D. Golberg).

¹ Permanent address: Laboratory of Non-Equilibrium Electronic Processes, Institute of Solid State Physics, Chernogolovka 142432, Russia.

contrast, NTs simultaneously composed of B, C and N atoms and exhibiting a limited number of layers have so far been unknown. In addition, all the B–C–N NTs reported to date have typically been observed as undulating, poorly graphitized multi-walled tubular fibers with numerous wall and core defects [2–17]. There has also been no consensus with respect to the atom distribution in multi-walled B–C–N NTs: contradicting models of definite phase (C and BN) separation, i.e. sandwich-like structures and heterojunctions [7,9,10,17, 28], and composite B–C–N layers [2–6,8,12,17,30–32] have been considered.

The present work has been carried out in an attempt to address all the above-mentioned issues. For the first time, we have synthesized perfectly ordered, straight and long (1–2 μm) B–C–N NTs with very few layers (typically 2–4) and studied their morphologies, chemical compositions and transport properties in three different types of microscopes as described below.

2. Experimental

The NTs were prepared in an induction furnace under a constant N_2 flow of 3.2 l/min [12–15,25,32]. A graphite crucible with mounted layers of B_2O_3 , Au_2O_3 and CVD-grown C NTs was heated gradually to 1950 K, held at 1950 K for 30 min and cooled down to room temperature over 2 h. The mixture of oxide powders and C NTs were physically separate from each other within the crucible to prevent embedding of the final product in the liquid bath created by the oxides under heating. This significantly increased the yield of extracted tubes.

The powder product (~ 50 mg) was collected from the crucible, milled and dispersed into CCl_4 . After ultrasonic treatment a few drops of the solution were dripped onto a C-coated-Cu grid (for high-resolution transmission electron microscopy (HRTEM) analysis) and onto a Ni mesh (for transport measurements). A 300 kV JEOL-3000F field-emission HRTEM and a 300 kV JEOL-3100FEF field-emission energy-filtered TEM (Omega filter) were used for atomic structure analysis and elemental mapping, respectively.

The elemental map acquisitions were performed using a 3 window procedure (2 pre-edge and 1-post edge energy filtered images were taken). The window energy shifts for the 1st, 2nd pre-edges, and the post-edge were, respectively, set as follows: for B (K-edge at 188 eV) – 28, 10, and 10 eV; for C (284 eV) – 26, 10, and 10 eV; for N (401 eV) – 28, 10, and 10 eV. The slit width of the Omega filter was adjusted to 20 eV. The spatial resolution of the energy-filtered images was estimated to be ~ 0.5 nm. Chemical compositions of the tubes were analyzed using an electron energy-loss spectrometer (EEL) ‘Gatan 766’ and an energy-dispersive X-ray (EDX) spectrometer ‘Noran Instruments’. Two-terminal transport measurements were performed in a Fresnel projection microscope [33]. We narrowed the gap between the sharp tungsten tip of the microscope and the tip-end of a free-standing individual NT bundle until a contact current was detected. The two-probe I–V characteristic of the bundle was then obtained by gradually changing the tip bias and measuring the current in the ‘tungsten tip – NT bundle – ground’ circuit. The X-, Y- and Z-tip movements were performed by inertial sliders and a piezotube for coarse and fine tip positioning, respectively. The microscope was placed in a vacuum chamber with a working pressure of 10^{-9} Torr.

3. Results

Figs. 1a–c show representative HRTEM micrographs of the thinnest double-walled NTs. Individual tubes (Fig. 1a); those assembled in thin bundles (Fig. 1b) and those in thick bundles (Fig. 1c) were normally observed. Representative EEL spectra taken from an individual four-shelled tube and from a thick tube bundle are shown in Figs. 2a,b, respectively. Both spectra are characteristic of a B–C–N material with definite core-loss K-edges at 188, 284, and 401 eV, corresponding to the B, C, and N signals, respectively. The sharp π^* -peaks on the left-hand side of the edges and the well-defined σ^* -bands on the right-hand sides are the fingerprints of the sp^2 -hybridized B, C and N atoms.

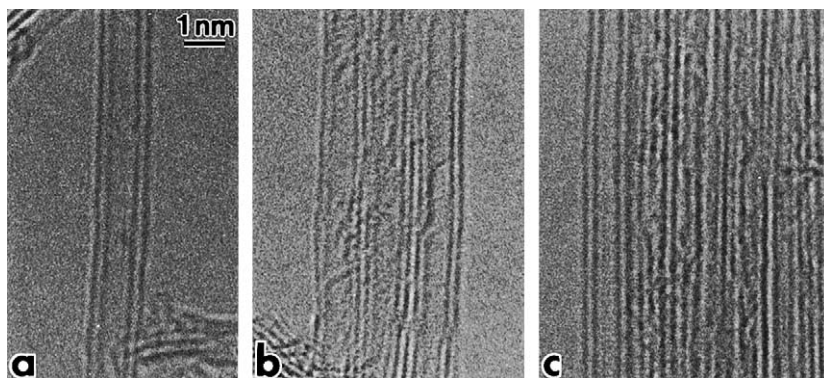


Fig. 1. Representative HRTEM images of the thinnest double-walled NTs: (a) an individual NT; (b) assembled in a thin bundle; (c) packed in a thick bundle.

There was sufficient microscopic evidence that the present B–C–N NTs had grown from the starting C NTs through templating, in line with our previous considerations [12–17,25]. The microscopic mechanism and growth kinetics are not yet well understood, although we frequently observed B–C–N NTs attached to the starting C NT templates. Metallic Au, which was a result of gold oxide decomposition during heating at 433 K, did not adhere to the tubular structures; no Au fillings or clusters were found within the grown NTs. Instead, Au nanocrystals were frequently encapsulated into by-product BN and B–C–N nanoparticles after the syntheses, as revealed by combined EEL and EDX analyses.

Figs. 3a,b depict the energy-filtered TEM images of an individual four-layered and a two-layered B–C–N NT. All three (B, C, and N) maps were successfully recorded for the four-layered tube (Fig. 3a). However, we were unable to record the N-map for the thinnest tube in Fig. 3b, since its intensity was too weak. In addition, the tubular morphology in Fig. 3b deteriorated dramatically due to the electron beam damage after consecutive B- and C-map acquisition as shown on the right-hand side zero-loss image in Fig. 3b. Figs. 3c,d quantitatively specify the B- and C-map contrast intensity profiles across the four-walled tube and along the double-walled tube previously shown in Figs. 3a,b, respectively.

Fig. 4 shows zero-loss and energy-filtered images of the two-layered B–C–N NTs assembled in

a bundle. For comparison, images of a wavy disordered B–C–N NT are also depicted in the figures (lower section). The morphology of the latter tube still resembles that of the starting CVD C template used for the synthesis. The difference in normalized B, C and N contrast brightness between the two nanostructures is obvious in Fig. 4.

Images of a representative B–C–N NT bundle (before (a) and after (b) I–V measurements), as revealed by Fresnel projection microscopy, together with measured I–V characteristics are shown in Figs. 5a–c. Importantly, the bundle was free-standing (Fig. 5a), i.e. it was supported by the substrate (a C-rich B–C–N NT residue mounted onto a Ni grid) from one side only. This is crucial for the current measurements since it allows us to completely exclude the effects of current leakage through the substrate. The shape of the I–V curves in Fig. 5c is characteristic of a semiconductor with ~ 1 eV band gap. Three consecutive representative curves are shown in Fig. 5c (sweeps 1, 2 and 3), which display good reproducibility.

4. Discussion

4.1. EEL spectra

Quantification of the EEL spectra depicted in Figs. 2a,b gave the following B, C, N atomic ratios within the nanostructures: individual four-shelled NT – B – 0.55 ± 0.08 ; C – 1.00 ± 0.00 ; and N –

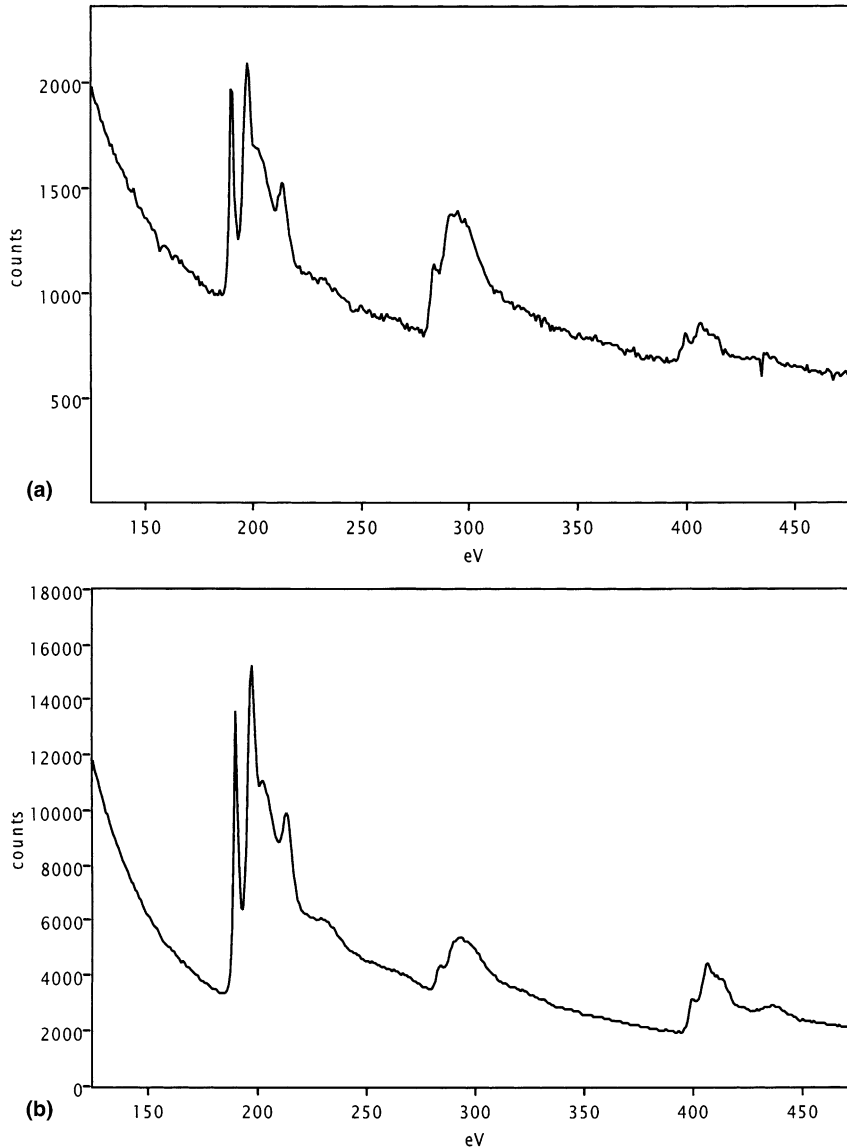


Fig. 2. Representative EEL spectra taken from: (a) an individual four-walled NT; (b) double-walled NTs packed into a rope. The core-loss K edges of B, C and N are visible at 188, 284 and 401 eV, respectively.

0.60 ± 0.09 ; bundle of NTs B – 0.79 ± 0.14 ; C – 0.48 ± 0.07 ; and N – 1.00 ± 0.00 . The cross-sections involved in the computation were calculated with the usual σ -K hydrogenic model [2]. In addition, we found that the relative B/C/N ratios marginally varied from one tube to the next and from one bundle to the next. It is worth noting that the observed C contents are not primarily due to

contamination of the inner core or external shells with a C residue: the HRTEM images of the B–C–N NTs (Figs. 1–3) look nearly perfectly clean.

Keeping in mind the pre-existing beliefs on the dominant trend for BN and C shell separation via organization into so-called sandwich-like structures [7,9,10,17,28] let us a priori assume the simple case of an equal number of BN and C shells for

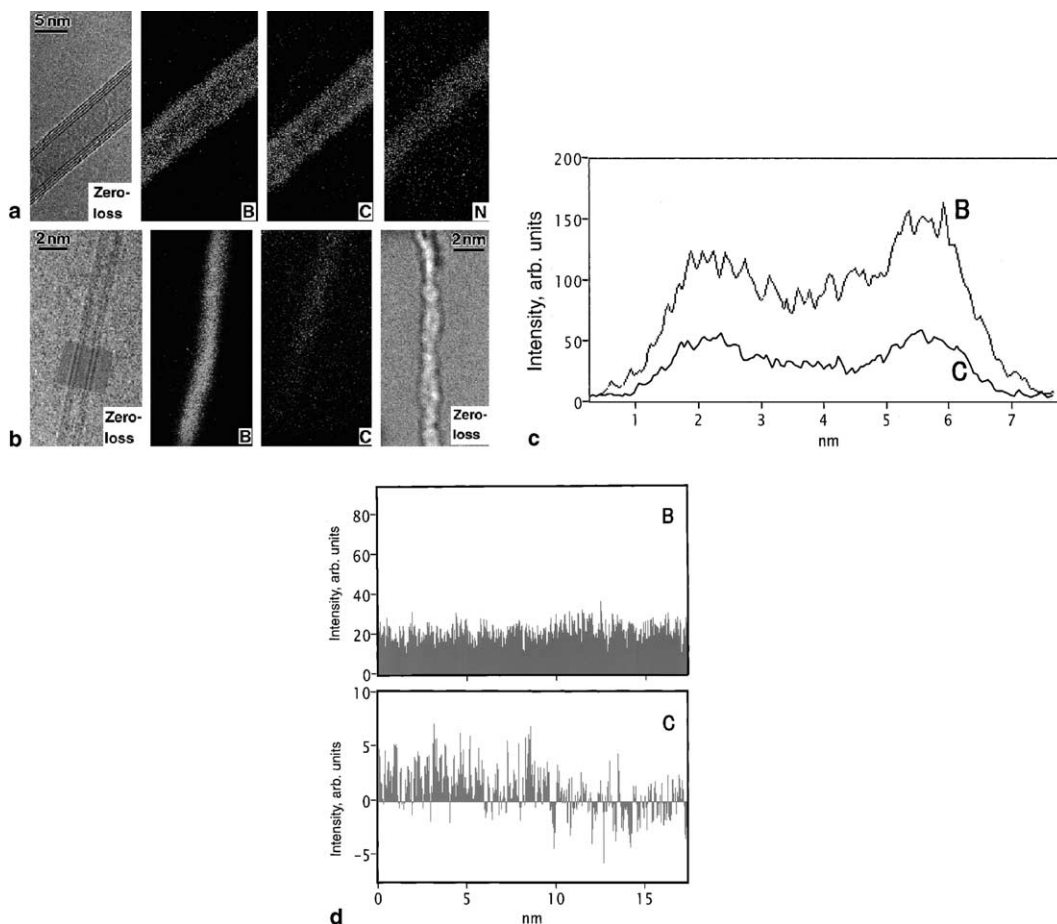


Fig. 3. Zero-loss and energy-filtered TEM images of (a) an individual four-walled B-C-N NT; (b) the thinnest individual double-walled B-C-N NT. We were unable to record an N-map in (b) due to its low intensity and tube damage due to the electron beam irradiation during the acquisition as shown on the right-hand side of the TEM image in (b). The long ($\sim 1 \mu\text{m}$) free-standing NT in (b) was blurred during study leading to noisy HRTEM contrast. Therefore, its exact two-walled morphology was confirmed by taking a HRTEM image at the bottom part of the tube shown in the inset. (c) The B- and C-elemental map contrast intensity profiles across the four-walled NT (from left to right) shown in (a); and (d) along the double-walled NT (from top to bottom) shown in (b). See text for details.

a given even-number-shelled NT (half of the shells – pure C; the other half – pure BN). Then the corresponding composition ratio in this case should be B – 0.50, N – 0.50 and C – 1.00. These values indeed look close to those measured for the four-shelled tube (Fig. 2a) within the estimated experimental error of $\sim 20\%$ (the error arises due to uncertainties in the background subtraction). However, one can argue that the shells may be composed of a stoichiometric BC_2N phase widely discussed in the literature [2,3,6,10,29]. Thus the

EEL data alone, routinely taken into account in most previous works [2–17], do not shed any light on whether the B-C-N NTs are composed of phase-separated BN and C shells and/or domains or complex B-, N-, and C-containing layers.

4.2. Elemental mapping

Fortunately, the energy-filtered spatially resolved TEM data presented in this Letter gave us a single answer: The present tubular shells typically

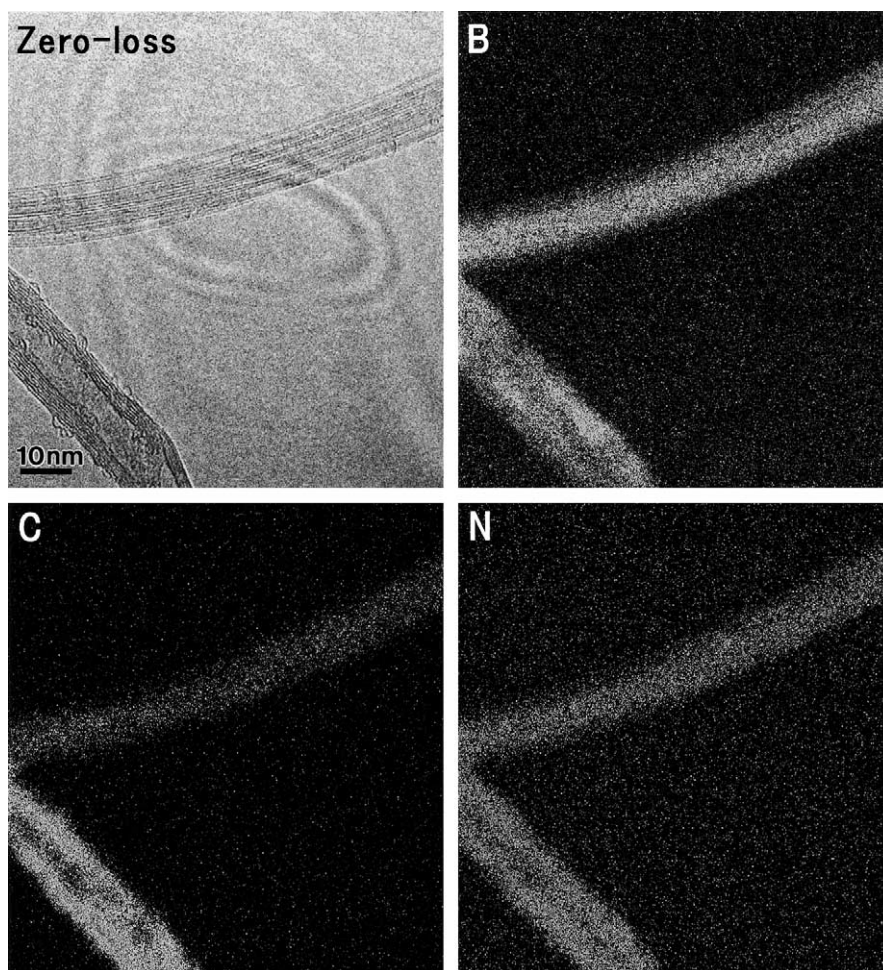


Fig. 4. Zero-loss and energy-filtered TEM images of a double-walled B–C–N NT bundle and an individual undulating disordered B–C–N NT whose morphology resembles that of a starting CVD C NT template. The ring pattern in the background of the zero-loss image is due to gain variations between pixels of a charge couple device used for taking digital TEM image. See text for further details.

contain all three species, namely, B, C and N, which are somehow assembled within the graphitic layers, rather than separating into well-defined pure C and BN shells and/or domains, or BN-rich and C-rich islands of sub-nanometer size, as reported in previous papers [7,9,10,15,17,28], where the NTs have been prepared via different synthetic routes. In fact, no basic trend for BN and C domain separation is visible in Figs. 3a,b. However, we note that the spatially resolved B-map is slightly wider than that of C in Fig. 3a; this implies that the outermost layer/layers of the four-walled NT may be enriched in BN and depleted in C. Fig.

3c verifies these statements quantitatively: the B- and C-map contrast intensity profiles across the four-walled tube perfectly correlate, and the B-intensity dominates on the periphery of the tube.

It is also noted that the C-map contrast in Fig. 3b is brighter in the upper tube part as compared to its lower part in accord with the corresponding C-content variations. This phenomenon is highlighted in Fig. 3d, where the corresponding B- and C-contrast intensity profiles along the double-walled tube (from its top to its bottom) are displayed. The B-contrast intensity is fairly uniformly distributed along the tube, whereas that of C

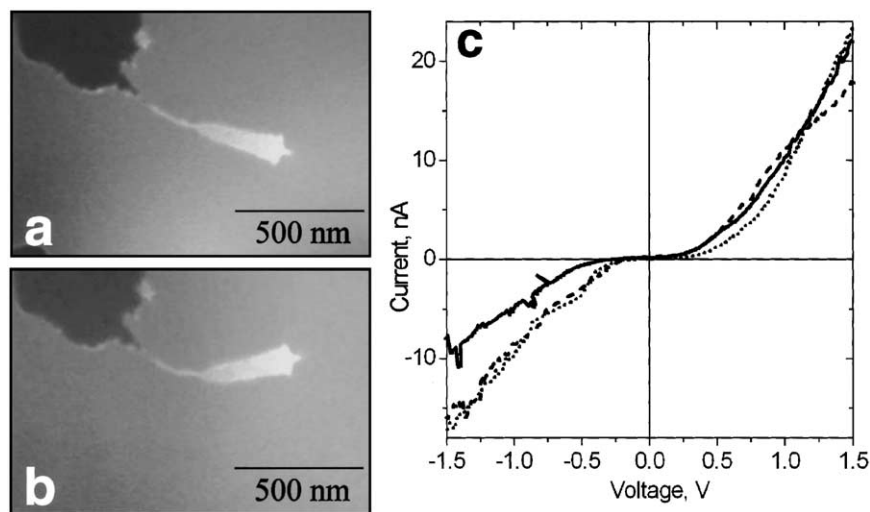


Fig. 5. Fresnel projection microscope images: (a) before transport measurements; (b) after transport measurements and (c) representative consecutive I–V curves of an individual B–C–N NT bundle. The curve key in (c) is as follows: solid line – 1st sweep; dashed line – 2nd sweep; and dotted line – 3rd sweep. All curves are characteristic of a semiconductor with an estimated band gap of ~ 1 eV.

markedly prevails in the upper tube part compared to its lower part (Fig. 3d). Clearly, the latter C-map contrast distribution would be inconsistent with a hypothesis of existence of one pure C and one pure BN shell but, conversely, favors the assemblage of two B–C–N layers with varying C-content along the tube. The close values of the B and N atomic ratios measured in some EEL spectra may also imply that stoichiometric BN islands may occasionally assemble within single C sheets, but the size of these islands should be well below the resolving power of the Omega filter TEM instrument (~ 0.5 nm). On the other hand, it is noted that in most cases the N-contents prevailed over those of B or vice versa. This implies that random spatial distribution of B and N in C sheets via formation of complex B–C–N, B–C and/or C–N containing six member rings could be presumed to exist.

This elemental distribution was also verified during energy-filtered experiments on the long and straight B–C–N NT bundle (Fig. 4). No evident separation of BN and C domains was seen; indeed, all three maps display fairly uniform brightness across and along the ropes with B/N overall intensities prevailing over C in line with the EELS data in Fig. 2b. Conversely, the other tubular

morphology, depicted in the lower section of Fig. 4 and resembling the starting CVD C template, displayed significant C enrichment at the expense of B and N.

All the above-mentioned results contradict much of the theoretical and experimental data presented so far for ternary B–C–N NTs [7,9,10,17,28], where BN and C shell and/or domain separation was highlighted as a key feature of the B–C–N system. In contrast, our spatially resolved energy-filtered data (Figs. 3 and 4) support the few theoretical predictions where substitution of B and N for C was assumed to occur within a single hexagonal sheet through formation of variable B–C–N compositions or stoichiometries [2–6,8,11,16,29–31]. We assume that this striking disagreement is related to the peculiarities and kinetics (rather than thermodynamics) of a given B–C–N NT synthesis. In our recent report on elemental mapping of thick aligned B–C–N tubular fibers we have shown that, generally, both forms of B/C/N coexistence may be realized, depending on the specific features of the synthesis: use of particular catalysts, reagents, temperature, vapor pressures, etc. [17]. For example, it is worth noting that, by comparison of the B- and C-map brightness intensities for the image of the disor-

dered tube in Fig. 4, one may randomly find C-poor, and, simultaneously, B-rich islands in the tube walls.

The role of a particular catalyst/promoter in synthesis of B–C–N and BN NTs from C NT templates has been mentioned before but is not yet understood [14,15,25], and it is far beyond the scope of this Letter. However, the stability of the few layer morphology in B–C–N NTs against the Au₂O₃ oxide-promoting synthesis is striking. Stable single- and/or double-walled morphologies were noted both in C and binary BN systems [21–27] but have never been mentioned for ternary B–C–N tubes, which so far have not displayed any selective criteria for choosing the number of grown layers [2–17]. The correct interpretation becomes even more complex given that we did not notice any direct Au impact on the growth process during careful HRTEM study: no encapsulated Au clusters or wires, unlike in MoO₃-promoted synthesis [25], or Au atoms at the growing tube edges, as in the case of PbO-promoted synthesis [25]. Instead, Au was mostly found to reside within numerous BN and B–C–N nanoparticles observed as a by-product. This additional result provides an opportunity to use such B–C–N and/or BN particle shells as Au cluster protection shields or nano-bearings.

4.3. Transport properties

To date there have been a few theoretical predictions that layered B–C–N materials may display semiconducting properties intermediate between metallic C NTs and dielectric BN NTs [3,29]. Liu et al. [29] predicted a 2.0 eV band gap for a BC₂N stoichiometric sheet, while Zhu et al. [31] calculated a 0.2 eV gap for a BCN layered network, a value which looked quite small given to the fraction of C present. There has been an experimental estimate of the band gap in a mat of ternary B_{0.34}C_{0.42}N_{0.24} undulating highly defective CVD tubular fibers using photoluminescence, stated to be around 1.0 eV [11]. The value of the band gap elucidated in the present Letter for an individual straight perfectly ordered B/N-rich B–C–N NT bundle (Figs. 2b and 4) was close to ~1 eV. The small value of the band gap is connected with the

global reduction of the ionicity of the B–C–N NT network as compared to pure BN NTs (band gap of ~5.5 eV [19]) whose transport properties have been very recently measured by Cumings and Zettl [34]. The detailed analysis of the I–V curves (Fig. 5) as well as precise band gap measurements and field emission properties of the present B–C–N NTs will soon be published elsewhere.

Finally, it is worth noting that due to significant fraction of B/N present in the semiconducting B–C–N bundles they are presumed to have higher oxidation resistance [35] and thermal stability than semiconducting pure C NTs. This is of prime importance for applications.

5. Conclusions

The few layer (2–4) morphology was found to be a stable configuration in the B–C–N NT system. Perfectly ordered long and straight B–C–N NTs with a limited number of defect-free layers synthesized by reacting C NT templates, boron oxide and gold oxide in a nitrogen flow at ~1950 K mainly exhibit a distribution of the constituent B, C and N atoms within the tubular layers rather than sandwich-like or island-like separation into BN and C shells and/or domains. Individual bundles of B–C–N NTs were measured to be semiconductors with an estimated band gap of ~1 eV.

Acknowledgements

The authors are grateful to Drs. T. Sato, K. Kurashima, M. Mitome and M. Terrones for valuable discussions, to Dr. H. Nejo for allowance and support in using the Fresnel projection microscope, and to Dr. J. Hester for reading the manuscript and providing useful suggestions.

References

- [1] S. Iijima, O. Stéphan, *Nature* 354 (1991) 56.
- [2] O. Stephan, P.M. Ajayan, C. Colliex, Ph. Redlich, J.M. Lambert, P. Bernier, P. Lefin, *Science* 266 (1994) 1683.

- [3] Z. Weng-Sieh, K. Cherrey, N.G. Chopra, X. Blase, Y. Miyamoto, A. Rubio, M.L. Cohen, S.G. Louie, A. Zettl, R. Gronsky, *Phys. Rev. B* 51 (1995) 11229.
- [4] M. Terrones, A.M. Benito, C. Manteca-Diego, W.K. Hsu, O.I. Osman, J.P. Hare, D.G. Reid, H. Terrones, A.K. Cheetham, K. Prassides, H.W. Kroto, D.R.M. Walton, *Chem. Phys. Lett.* 257 (1996) 576.
- [5] Ph. Redlich, J. Loeffler, P.M. Ajayan, J. Bill, F. Aldinger, M. Ruhle, *Chem. Phys. Lett.* 260 (1996) 465.
- [6] Y. Zhang, H. Gu, K. Suenaga, S. Iijima, *Chem. Phys. Lett.* 279 (1997) 264.
- [7] Y. Zhang, K. Suenaga, C. Colliex, S. Iijima, *Science* 281 (1998) 973.
- [8] R. Sen, B.C. Satishkumar, A. Govindaraj, K.R. Harikumar, G. Raina, J.P. Zhang, A.K. Cheetham, C.N.R. Rao, *Chem. Phys. Lett.* 287 (1998) 671.
- [9] K. Suenaga, F. Willaime, A. Loiseau, C. Colliex, *Appl. Phys. A* 68 (1999) 301.
- [10] Ph. Kohler-Redlich, M. Terrones, C. Manteca-Diego, W.K. Hsu, H. Terrones, M. Rühle, H.W. Kroto, D.R.M. Walton, *Chem. Phys. Lett.* 310 (1999) 459.
- [11] J. Yu, J. Ahn, S.F. Yoon, Q. Zhang, Rusli, B. Gan, K. Chew, M.B. Yu, X.D. Bai, E.G. Wang, *Appl. Phys. Lett.* 77 (2000) 1949.
- [12] D. Golberg, Y. Bando, W. Han, K. Kurashima, T. Sato, *Chem. Phys. Lett.* 308 (1999) 337.
- [13] D. Golberg, Y. Bando, L. Bourgeois, K. Kurashima, T. Sato, *Carbon* 38 (2000) 2017.
- [14] D. Golberg, Y. Bando, K. Kurashima, T. Sato, *Diam. Rel. Mater.* 10 (2001) 63.
- [15] Y. Bando, D. Golberg, M. Mitome, K. Kurashima, T. Sato, *Chem. Phys. Lett.* 346 (2001) 29.
- [16] W. Han, J. Cumings, A. Zettl, *Appl. Phys. Lett.* 78 (2001) 2769.
- [17] D. Golberg, Y. Bando, M. Mitome, K. Kurashima, N. Grobert, M. Reyes-Reyes, H. Terrones, M. Terrones, *Chem. Phys. Lett.*, in press.
- [18] J.W.G. Wildöer, L.C. Venema, A.G. Rinzler, R.E. Smalley, C. Dekker, *Nature* 391 (1998) 59.
- [19] X. Blase, A. Rubio, S.G. Louie, M.L. Cohen, *Europhys. Lett.* 28 (1994) 335.
- [20] V.H. Crespi, M.L. Cohen, A. Rubio, *Phys. Rev. Lett.* 79 (1997) 2093.
- [21] A. Thess, R. Lee, P. Nikolaev, H. Dai, P. Petit, J. Robert, C. Xu, Y.H. Lee, S.G. Kim, A.G. Rinzler, D.T. Colbert, G.E. Scuseria, D. Tomanek, J.E. Fisher, R.E. Smalley, *Science* 273 (1996) 483.
- [22] J.L. Hutchison, N.A. Kiselev, E.P. Krinichnaya, A.V. Krestinin, R.O. Loutfy, A.P. Morawsky, V.E. Muradyan, E.D. Obraztsova, J. Sloan, S.V. Terekhov, D.N. Zaharov, *Carbon* 39 (2001) 761.
- [23] J. Cumings, A. Zettl, *Chem. Phys. Lett.* 316 (2000) 211.
- [24] T. Laude, Y. Matsui, A. Marraud, B. Jouffrey, *Appl. Phys. Lett.* 76 (2000) 3239.
- [25] D. Golberg, Y. Bando, *Appl. Phys. Lett.* 79 (2001) 415.
- [26] A. Loiseau, F. Willaime, N. Demoncy, G. Hug, H. Pascard, *Phys. Rev. Lett.* 76 (1996) 4737.
- [27] R.S. Lee, J. Gavilett, M.L. de la Chapelle, A. Loiseau, J.L. Cochon, D. Pigache, J. Thibault, F. Willaime, *Phys. Rev. B* 64 (2001) 1405.
- [28] X. Blase, J.-Ch. Charlier, A. De Vita, R. Car, *Appl. Phys. A* 68 (1999) 293.
- [29] A.Y. Liu, R.M. Wetzcovitch, M.L. Cohen, *Phys. Rev. B* 39 (1988) 1760.
- [30] M. Kawaguchi, *Adv. Mater.* 9 (1997) 615.
- [31] H.-Y. Zhu, D.J. Klein, N.H. March, A. Rubio, *J. Phys. Chem. Sol.* 59 (1998) 1303.
- [32] W. Han, Y. Bando, K. Kurashima, T. Sato, *Appl. Phys. Lett.* 73 (1998) 3085.
- [33] V. Thien Binh, P. Vincent, F. Feschet, J.-M. Bonard, *J. Appl. Phys.* 88 (2000) 3385.
- [34] J. Cumings, A. Zettl, in: H. Kuzmany et al. (Eds.), *Electronic Properties of Molecular Nanostructures*, AIP Conf. Proc. Ser., 2001, New York, p. 577.
- [35] D. Golberg, Y. Bando, K. Kurashima, T. Sato, *Scripta Mater.* 44 (2001) 1561.